applied sciences

MDPI

Article

Modeling Power Flows and Electromagnetic Fields Induced by Compact Overhead Lines Feeding Traction Substations of Mainline Railroads

Konstantin Suslov [1,2,*], Andrey Kryukov [2,3], Ekaterina Voronina [3] and Ilia Fesak [3]

[1] Department of Hydropower and Renewable Energy, National Research University "Moscow Power Engineering Institute", Moscow 111250, Russia
[2] Department of Power Supply and Electrical Engineering, Irkutsk National Research Technical University, Irkutsk 664074, Russia
[3] Department of Electric Power Engineering of Transport, Irkutsk State Transport University, Irkutsk 664074, Russia
* Correspondence: dr.souslov@yandex.ru; Tel.: +791-48-704-673

Abstract: The ongoing re-equipment of electric power systems is based on the use of smart grid technologies. Among the key tasks that are solved on this basis are increasing the capacity of power transmission lines, reducing losses, and improving power quality. To address these issues, one can use compact power transmission lines. Such lines are notable for their complex split-phase designs and close together placement of current-conducting parts, so as to keep the distance to a permissible minimum, which is achieved by the use of insulating spacers. This article reports the results of computer-aided simulations performed for a standard railroad power supply system, the traction substations of which were connected to 220 kV networks through compact overhead lines (COHLs). The purpose of the study was to calculate the values of quantitative metrics that measure power quality and energy efficiency as well as electromagnetic safety. Modeling was performed in the three-phase reference frame with the use of techniques and algorithms implemented in the Fazonord software package. We considered a power supply system with 25 kV overhead contact systems. It was assumed that the external network used three different designs of COHLs: with coaxial, linear, and sector-shaped arrangements of conductors. Based on the results obtained, we concluded that (1) when using COHLs, the voltages on bow collectors of electric rolling stock were stabilized and did not exceed permissible limits; (2) losses in the traction network were reduced; and (3) the parameters of power quality and electromagnetic safety conditions in external power supply systems of railroads were improved, if judged in terms of electric and magnetic field strengths. Out of the eight types of COHLs considered, compact lines with the three-segment and concentric arrangement of conductors had the best performance, and the use of COHLs with the vertical arrangement of conductors made it possible to reduce electric field strengths. However, the designs of such transmission lines are quite complex and entail higher construction costs.

Keywords: compact overhead lines; traction power supply systems; simulation; power quality and energy efficiency; electromagnetic fields

check for updates

Citation: Suslov, K.; Kryukov, A.; Voronina, E.; Fesak, I. Modeling Power Flows and Electromagnetic Fields Induced by Compact Overhead Lines Feeding Traction Substations of Mainline Railroads. *Appl. Sci.* **2023**, *13*, 4249. https://doi.org/10.3390/app13074249

Academic Editors: Frede Blaabjerg and Gaetano Zizzo

Received: 22 January 2023
Revised: 23 February 2023
Accepted: 23 March 2023
Published: 27 March 2023

Copyright: © 2023 by the authors. Licensee MDPI, Basel, Switzerland. This article is an open access article distributed under the terms and conditions of the Creative Commons Attribution (CC BY) license (https://creativecommons.org/licenses/by/4.0/).

1. Introduction

Electrified railroads are large and spatially dispersed consumers of electricity, and they require a reliable and efficient power supply for the traction of trains and the fixed-site facilities of transport infrastructure. To address these issues and stay relevant in today's context, technological upgrades to electric power systems (EPS) are being carried out, which are based on the adoption of smart grid technologies. One important area of the adoption of these technologies is the use of compact power transmission lines, which are characterized by their complex split-phase designs and close together placement of current-conducting

parts. The distance between them is kept to a permissible minimum, which is achieved by the use of insulating spacers.

A large body of research, published in this country and abroad, has addressed the issues of design and analysis regarding power flows in electric power systems equipped with COHLs. A detailed presentation of the basic theoretical aspects of building COHLs is available in books [1,2]. Articles [3,4] describe power flow considerations related to compact 220 kV lines. Study [5] discusses the issues of design in high-voltage COHLs. The results of the COHL capacity assessment were reported in [6]. The issues of reliability, economic performance, and quality of COHLs are discussed in article [7]. Papers [8,9] deal with design features specific to COHLs. Novel engineering solutions for power transmission links, including COHLs, are reported on in research monograph [10]. Articles [11,12] evaluate the effectiveness of the use of compact controlled transmission lines. In [13] a design of a compact quadruple circuit 500 kV transmission line is presented. This was proposed in order to increase the cross-arm length of the ground steel wire to improve the shielding angle, which reduces the maximum peak current of lightning that can strike the phase wire. In article [14], a software tool was developed for modeling compact power transmission lines via finite element analysis, as well as for calculating the surface electric field distribution. The results indicated that the maximum electric field strength decreased by nearly 36% to 25 kV/cm from 39 kV/cm. In [15], methods for increasing the transfer capacity of 35–220 kV transmission lines through the use of novel small-sized tower designs are proposed. The authors developed original techniques for determining the inductive reactance and capacity admittance values of the proposed COHLs. Article [16] deals with the study of induced voltage on AC power lines. The results of the study attested to the fact that by relying on COHLs, it was possible to reduce the induced voltage on DC power transmission lines as the induced voltage decreased from 24 to 17 kV, given a distance of 40 m between the lines. Study [17] discusses the possibility of increasing the transfer capacity of 35–220 kV transmission lines by placing phases closer together and splitting them. It was shown that the use of insulating cross-arms can increase the transmitted power as well as reduce the overall size of the transmission line and the right-of-way area. Article [18] investigated alternatives to parallel lines in terms of the magnetic flux density level of conductors. The design presented in the article exhibited the highest levels of magnetic flux density. Study [19] examined 115 kV three-phase compact transmission lines. Article [20] reports the results of the electric field analysis of a small-sized 150 kV transmission line. The results indicated that the highest electric field strength reached 6 kV/m, which is in compliance with the WHO standard (10 kV/m). Paper [21] dealt with tests of air gaps during pulse voltage discharge switching in a compact transmission line. It provided guidelines for the design and maintenance of extra-high voltage COHLs, which is useful for ensuring the reliability of electrical networks. Article [22] analyzed the difficulties that arise in large-capacity long-distance power transmission. The authors reported the results of preliminary research on the benefits of COHLs in terms of increased transmission capacity. Based on those studies, they proposed a concept of a flexible compact AC transmission system. Study [23] investigated the outage rate caused by lightning strikes on compact power transmission lines. To that end, design differences between compact and conventional power transmission lines were taken into consideration. Article [24] dealt with the magnetic field analysis of a 150 kV compact transmission line. The results indicated that the maximum magnetic field density around the 150 kV compact transmission line was 8.25 μT, which met the WHO standard (100 μT). In [25], methods for lightning protection of compact overhead power lines are presented. Article [26] discusses the engineering aspects of a new configuration of transmission line. The line was of a compact delta design, differing significantly from the standard flat horizontal configuration. Article [27] details the testing of the first small-scale 500 kV transmission line in China. A number of tests were conducted to investigate its characteristics. The electrical parameters, including positive and negative sequence impedances, matched the design values. In [28], it was shown that large-power compact overhead 500 kV transmission lines will contribute to significant

economic gains. In [29–32], several models of 500 kV compact transmission lines were described, including single-circuit and double-circuit ones. The results of the calculations confirmed that the application of COHLs can reduce the maximum surface field gradients as well as reduce the surge impedance, which leads to a significant increase in transfer capacity. The main characteristics of COHLs are reported in [30].

On the basis of the above review, we can conclude that the relevance of the study of load flows and electromagnetic fields of COHLs has been well-established. In the future, it will be possible to use COHLs in the networks feeding traction substations of mainline AC railroads. Against the backdrop of digitalization and the use of power in the transport sector, computer technologies should be utilized to assess the effectiveness of such engineering solutions. This can be implemented based on the integrated modeling of electric power systems and power supply systems of railroads using the three-phase (ABC) frame of reference [33]. Below are the results of research aimed at developing digital models of COHLs and determining the effectiveness of utilizing such transmission lines in 220 kV electrical networks that power traction substations.

This study contributes to the existing literature by providing the following:

- We propose original models of power systems and power supply systems for AC railroads, with such models enabling quantitative evaluation of efficacy and the application of COHLs for supplying power to traction substations;
- The approach adopted for the creation of these models stands apart from other approaches in that it is system-based and treats COHLs as inseparable from the power flows of a complex power system.
- In contrast to traditional methods based on a single-line representation, our models were built using the three-phase (ABC) reference frame, which provides the most adequate modeling of power system load flows with single-phase traction loads that create significant imbalances in the electrical networks that feed them.
- Dynamics changes in traction loads were captured by simulating the movement of trains along real-world rail track profiles.

2. Object of the Study

The simulations reported in this paper were performed in the Fazonord software package [33]. We considered a power supply system for a section of mainline railroad, including an external 220 kV network, four traction substations, and three areas between the substations (Figure 1). The simulation was carried out for two scenarios. In the first one, the 220 kV feeder network used standard lines (Figure 2) made of AS-600 wires, and in the second one, the power lines had a compact design (Figure 3). The COHLs investigated here fall into three groups: with coaxial, linear, and sector-shaped arrangements of conductors. We considered eight COHL designs. The coordinates of their conductors are shown in Figure 4.

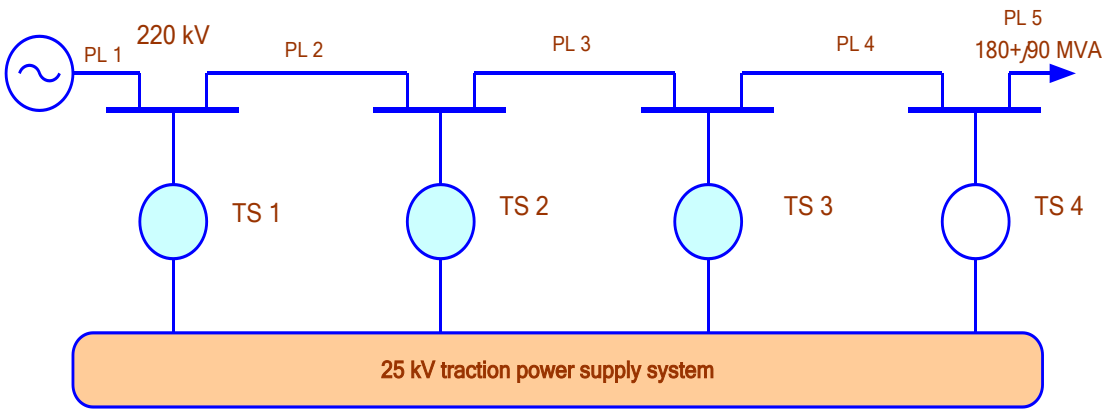


Figure 1. Network circuit: TS–traction substation.

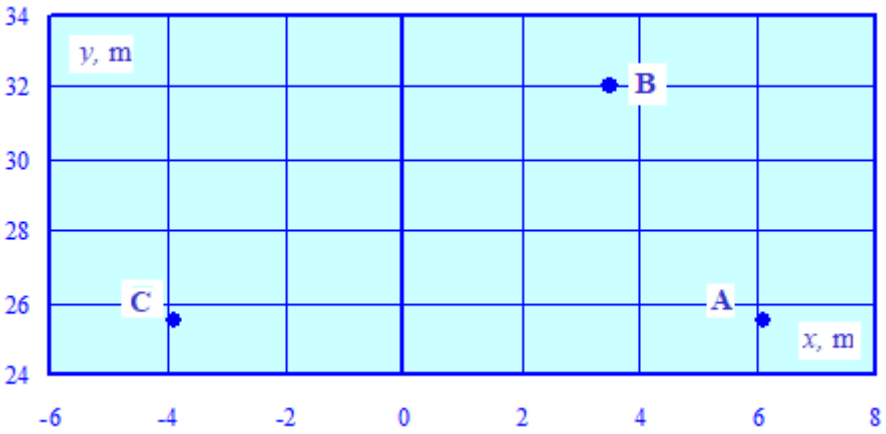


Figure 2. Coordinates of the arrangement of conductors of the power line of a standard design.

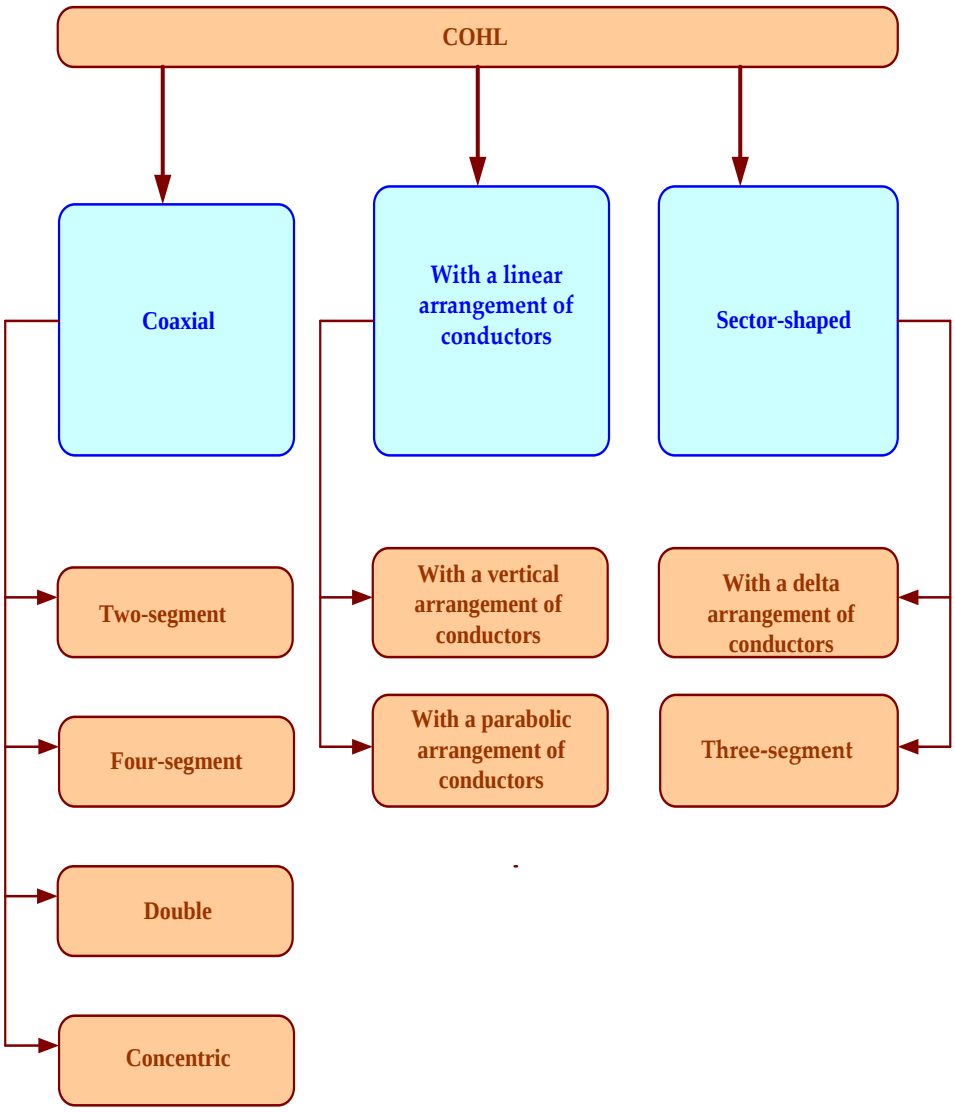


Figure 3. Classification of COHLs.

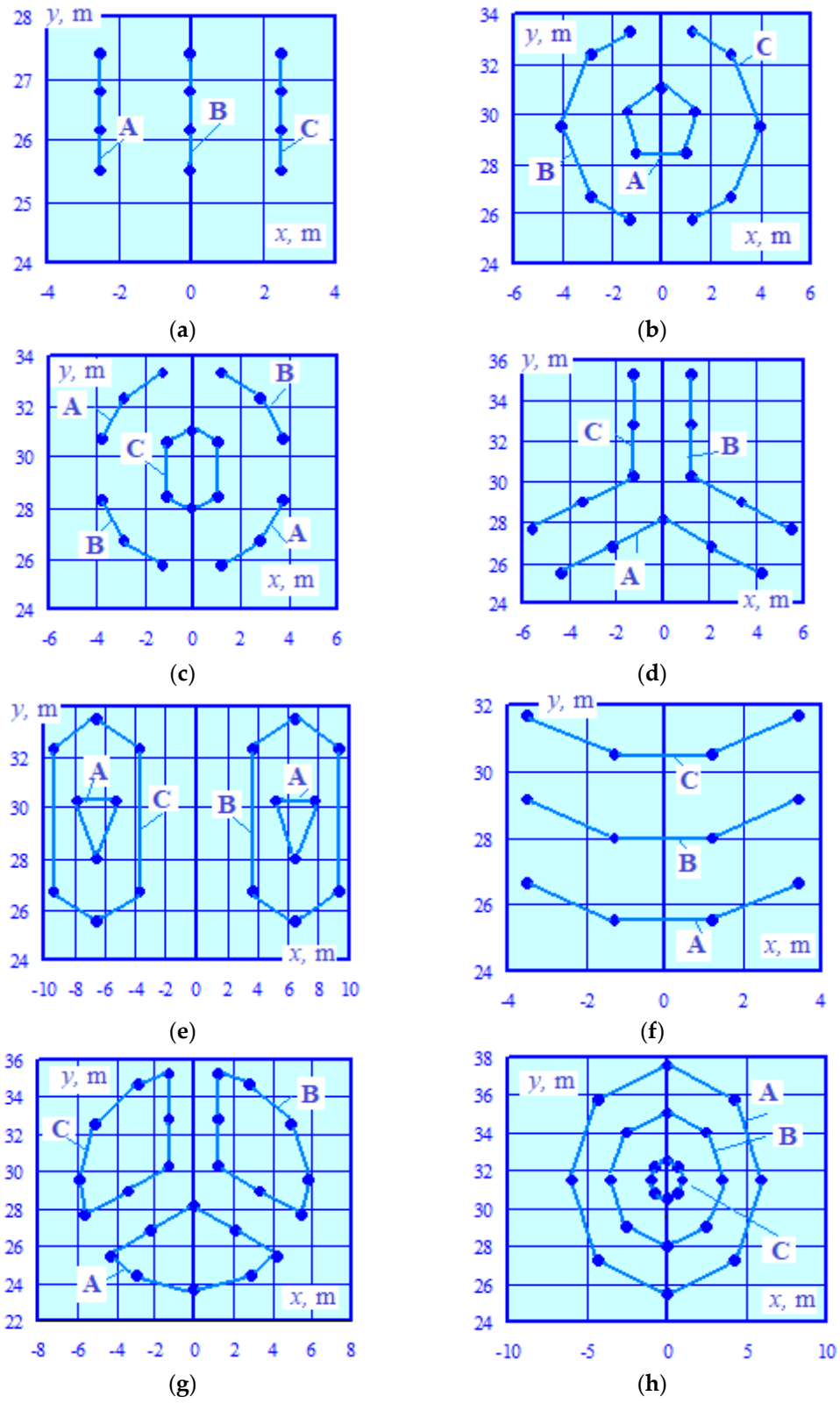


Figure 4. Coordinates of conductor arrangement for compact transmission lines: (**a**)—with a vertical arrangement of conductors, (**b**)—two-segment coaxial, (**c**)—four-segment coaxial, (**d**)—delta, (**e**)—double coaxial, (**f**)—parabolic, (**g**)—three-segment, (**h**)—concentric.

Compact power transmission lines are characterized by their unconventional arrangements of conductors and close together placement of phases, which keep the distance

between them to a permissible minimum. The distance is subject to technical limitations, which are determined by the following factors:

- Possible movement of conductors within the span due to wind;
- Non-synchronous galloping;
- Galloping during ice removal;
- Possible overvoltages and constraints on corona discharge.

Compact power transmission lines are built by bringing phase conductors closer together using in-span spacers made of insulating materials, such as polymer rod insulators. In this case, the distances between phases on the towers do not change.

Another way of building compact transmission lines is based on the use of special-purpose towers. When selecting the minimum allowable phase distances, switching overvoltages act as the limiting factor. Minimum cross-section values are limited by radio interference and corona losses.

In terms of their design, the investigated COHLs fall into three groups (Figure 3):

- Lines with a coaxial arrangement of conductors (Figure 4b,c,e,h);
- Power transmission lines with a linear arrangement of current-conducting parts (Figure 4a,e);
- Sector-shaped COHLs (Figure 4d,g).

In addition to obviously reducing right-of-way requirements, compact overhead lines lessen the impact of electromagnetic fields on the natural environment, increase the capacity of power transmission lines, and reduce power losses compared to conventional three-phase lines. These factors can be measured in quantitative terms by modeling COHLs using the three-phase frame of reference for different types of compact lines. The results of such modeling, performed in the Fazonord software package, are detailed below. Key differences between the presented findings and the results reported in the literature review of Section 1 include the following: load flow analysis of COHLs was carried out so as to take into account the significant unbalance caused by single-phase traction loads; simulations were performed for a series of load flows corresponding to the movement of traction loads in space.

3. Method and Results of Modeling

The main idea behind the method of modeling components for electric power plants and traction power supply systems (TPSS) in the phase frame of reference is the use of equivalent lattice circuits with a fully connected topology for power transmission lines, traction AC networks, and transformers [30]. Forming a lattice circuit presupposes the following:

(1) The presence of flat conductive homogeneous earth;
(2) Line wires that run parallel to each other and the ground surface;
(3) Consideration of conductor current return through the ground for power transmission lines and traction networks;
(4) Conductor radii that are small compared to the distances between current-carrying parts;
(5) The sequence of conductor numbering is determined by the order governing the arrangement of information about them;
(6) Positive directions of currents from the side external to the circuit component are assumed to be those directed towards (inside) the multi-conductor component;
(7) Potentials of the nodes are counted relative to the zero-ground potential.

Lattice circuit modeling of a multi-conductor line is performed in three steps. In the first step, an equivalent circuit with a fully connected topology is formed on the basis of self and mutual values of ohmic resistance and reactance of conductor-to-ground circuits. The second step involves calculating the self and mutual capacitances of the conductors and the third step deals with possible connections linking the ends of the conductors to

each other. The formation of the lattice circuit of the transformer is based on the equations of its electrical and magnetic state.

Our approach makes it possible to obtain models of almost all possible configurations of power transmission lines and power transformers, while taking into account the mutual-inductance coupling of conductors (transformer coils) with each other and the capacitances of line conductors. The resulting lattice circuit includes impedors (*RL* elements) whose ohmic resistance and reactance can have negative signs.

Thus, a multi-conductor system of n conductors, in which each conductor has mutual-inductance couplings with the others, can be substituted with an equivalent circuit made up of *RL*-branches that have a fully-connected topology. The number of these branches is $2n(2n\text{-}1)/2$, and their conductances are determined from the conductance matrix of the multi-conductor system.

The capacitance coupling of conductors is taken into account after processing the mutual-inductance couplings. The self and mutual capacity admittances of the conductors in the U-shaped equivalent circuit are added to the corresponding nodes and branches of the lattice circuit.

If the component has no links to the node of zero potential (ground), i.e., $\underline{z}_{k0} = \infty$ $k = 1...n$, the matrix $\underline{\mathbf{Y}}_{PC}$ is the n-fold degenerate, which does not prevent the model from being used in calculations. Adding capacity admittances to ground or connecting components that have connections to ground eliminates the degeneracy of the matrix.

The capacity admittances of the lattice circuit are determined from the potential coefficients of the first group of Maxwell's equations:

$$\mathbf{U} = \mathbf{AT} \tag{1}$$

$$\mathbf{T} = \begin{bmatrix} \tau_1 & \tau_1 & \dots & \tau_n \end{bmatrix}^{\mathrm{T}} \tag{2}$$

where **U**–n is the dimensional vector of conductor-to-ground voltages, **T** is the vector of conductor charges, and **A** is the matrix of potential coefficients of dimension $n \times n$.

Using the matrix of capacitance coefficients,

$$\mathbf{B} = \mathbf{A}^{-1} \tag{3}$$

the self- and mutual partial capacitances are calculated, and shunts are added to the nodes of the lattice circuit, whose conductances are determined by half of the corresponding self-capacitance. In addition, on each side of the conductor system, additional branches are formed with impedance values calculated by half the values of the corresponding mutual capacitances.

The self-impedances of power transmission line conductors are calculated from Carson's equations for the near range, with the addition of the internal resistance of the conductors. The external impedance is calculated as per the following expressions:

$$\underline{Z}_{\mathrm{ext}} = 0.001f + jf[0.01148 - 0.001256\ln(r\sqrt{0.02\sigma f})],\ \mathrm{Ohm/km}; \tag{4}$$

where f is the frequency, measured in Hz; r is the equivalent conductor radius (for steel-reinforced aluminum conductors, it is assumed to be 0.95 times the external radius of the conductor cross-section), measured in cm; and σ is the specific conductance of the homogeneous earth (or equivalent weighted average conductance), measured in S/m.

The internal resistance is different for different types of conductors. For steel-reinforced aluminum conductors, approximating approximate relationships are used:

$$R_{\mathrm{in}} = R_0(0.9 + 0.0063f^{0.755}),\ \mathrm{Ohm/km}; \tag{5}$$

$$X_{\mathrm{in}} = 0.001\left[\left(0.033 - 0.00107f^{0.83}\right)S + 1.07f^{0.83} - 13.5\right],\ \mathrm{Ohm/km}; \tag{6}$$

where R_0 is the resistance of 1 km of the conductor to direct current, measured in Ohm/km; f is the frequency, measured in Hz; and S is the cross-sectional area of the conductor, measured in mm^2.

For solid aluminum and copper conductors with a cylindrical cross-section, the internal resistance is calculated by approximate formulas, provided that $|qr| \leq 4$:

$$R_{\text{in}} = R_0(1 + 0.0049x^4 - 0.000035x^7), \text{ Ohm/km;} \tag{7}$$

$$X_{\text{in}} = R_0(0.125x^2 - 0.000613x^5), \text{ Ohm/km;} \tag{8}$$

$$\underline{q} = \sqrt{-j\omega\gamma_{\Pi}\mu_0};\ x = 0.01r\sqrt{\frac{7896f}{R_0S}} \tag{9}$$

where γ_{Π} is the specific conductance of conductor material; r is the conductor radius, measured in cm; and S is the cross-sectional area of the conductor, measured in mm^2.

For large values of x we use the ratio

$$R_{\text{in}} = X_{\text{in}} = \frac{R_0x}{2\sqrt{2}} \tag{10}$$

For steel wires and rails, we use the approximate expression

$$R_{\text{in}} = R_{50}\sqrt{0.02f},\ X_{\text{in}} = 0.75R_{\text{in}} \tag{11}$$

where R_{50} is the ohmic resistance for a frequency of 50 Hz.

The technique for load flow analysis of complex EPSs properly calculates the mutual electromagnetic effects in the near, intermediate, and far ranges of Carson's integral [34].

Mutual inductance M_{ik} is the central concept from which inductive effects are determined. It involves the instantaneous transmission of load flow changes of individual conductors throughout a multi-conductor system. When determining M_{ik}, we consider the conductor-to-ground circuits. For sine wave processes, the mutual inductance yields a proportional relationship between the current in the circuit that creates the magnetic field and the EMF induced in the other circuit.

$$\dot{\mathcal{E}} = -j\omega M_{ik}\dot{I}l = -\underline{Z}_{ik}\dot{I}l \tag{12}$$

where $\underline{Z}_{ik}$ represents the impedance of the mutual-inductance coupling between circuits i and k, referred to 1 km of the length of the interacting conductors of length l; and ω is the angular frequency.

Carson's formulas [34] are based on the correct solution of Maxwell's equations and allow the self- and mutual inductances of conductors to be determined. They can be used to find the external self-impedance of a straight-line conductor over a flat surface of the homogeneous earth, as well as the mutual impedance of two conductors, taking into account the ground return currents. There are approximate expressions for the near and far ranges that do not apply to the intermediate range. The alignment chart given in [35] can be used for this purpose, or one can use the direct calculation of the series to which the integral is reduced; in this case, to achieve a high calculation accuracy, it is sufficient to consider the 14 members of the series.

Accounting for the delay in EMF propagation becomes more complicated when calculating the effects for harmonics as it becomes necessary to apply Carson's solutions to the intermediate and far ranges, and to use the long-line equations as steady-state equations.

The Fazonord package forms an equivalent lattice circuit of a multi-conductor system based on expressions for the self- and mutual impedances of individual conductors. Therefore, we need a high-performance algorithm for implementing Carson's formulas that will provide sufficient accuracy for practical purposes in the near, intermediate, and far ranges.

In Carson's approach where the actual earth is replaced by a plane homogeneous solid, the method of mirror images is adjusted for its finite conductivity; in this case, the external self-impedance of a rectilinear conductor of small diameter and the mutual impedance of two parallel conductors are calculated as per the following formula [34]:

$$\underline{Z}_{ik} = \frac{j\omega\mu_0}{2\pi}\left(\ln\frac{r_{ik}{}'}{r_{ik}} + \underline{F}_{ik}\right) = j1.2566\cdot 10^{-6} f\left(\ln\frac{r_{ik}{}'}{r_{ik}} + \underline{F}_{ik}\right) \tag{13}$$

where ω is the angular frequency, s^{-1}; $\mu_0 = 4\pi\cdot 10^{-7}$ H/m; $r_{ik}{}'$ is the distance between the conductor k and the mirror image of the wire i, measured in m; r_{ik} is the distance between conductors i and k, measured in m.

If we do not consider ground bias currents, the summand $\underline{F}_{ik}$ determining the addition due to the finite ground conductivity can be found as follows:

$$\begin{gathered}\underline{F}_{ik} = 0.5 - \ln(\lambda r) - j\tfrac{\pi}{4} - \\ -\sum_{n=1}^{\infty}(-1)^n \tfrac{(r/2)^{2n} e^{jn\pi/2}}{n!(n+1)!}\times\left[\left(\ln(\lambda r) - m_n + j\tfrac{\pi}{4}\right)\cos(2n\theta) - \theta\sin(2n\theta)\right] - \\ -2\sum_{n=1}^{\infty}(-1)^n \tfrac{r^{2n-1}e^{j(2n-1)\pi/4}\cos[(2n-1)\theta]}{1^2\cdot 3^2\cdot 5^2\cdot\ldots\cdot(2n-1)^2\cdot(2n+1);} \\ m_n = 1 + \tfrac{1}{2} + \ldots + \tfrac{1}{n+1} - \tfrac{1}{2(n+1)}; \\ r = r_{ik}{}'\sqrt{\tfrac{\omega\mu_0}{\rho}} = 2.8099\cdot 10^{-3}\cdot r_{ik}{}'\sqrt{\tfrac{f}{\rho}}; r_{ik}{}' = \sqrt{(x_i - x_k)^2 + (y_i + y_k)^2}; \\ \theta = \operatorname{arctg}\tfrac{x_i - x_k}{y_i + y_k},\end{gathered} \tag{14}$$

where f is the frequency, measured in Hz; ρ represents ground resistivity, measured in Ohm-m; and λ = 0.890536209; (x_i, y_i), (x_k, y_k) represents the coordinates of conductors, m.

In deriving expressions (13) and (14), the y-axis direction is chosen to be vertically upward, the x-axis is perpendicular to the conductor axes, and the z-axis is opposite to the positive current direction. The origin of the coordinates is on the surface of the earth.

In the near range, when $r \le 0.25$ an approximate expression of the following form is used for Formula (14):

$$\underline{F}_{ik} = -0.077216 - \ln\frac{r}{2} + \frac{\sqrt{2}}{3}r\cos\theta - j\left(\frac{\pi}{4} - \frac{\sqrt{2}}{3}r\cos\theta\right) \tag{15}$$

for the far range that meets the condition $r \ge 5$, the following formula is used:

$$\underline{F}_{ik} = \frac{\sqrt{2}}{r}\left[(1-j)\cos\theta + j\frac{\sqrt{2}\cos 2\theta}{r} - (1+j)\frac{\cos 3\theta}{r^2} + (1-j)\frac{3\cos 5\theta}{r^4}\right] \tag{16}$$

when $i = k$ and $r \le 0.2$, Expression (13) corresponds to the external impedance of the conductorш

$$\begin{gathered}\underline{Z}_{\mathcal{B}\mathcal{H}ew} = \tfrac{\omega\mu_0}{8} + j\tfrac{\omega\mu_0}{2\pi}\ln\left(\tfrac{1}{r_{ii}}\tfrac{2}{\gamma}\sqrt{\tfrac{e\rho}{\omega\mu_0}}\right) \\ = \tfrac{\omega\mu_0}{8} + j\tfrac{\omega\mu_0}{2\pi}\ln\left(\tfrac{1.8514}{r_{ii}}\sqrt{\tfrac{\rho}{\omega\mu_0}}\right), \text{ Ohm}/m,\end{gathered} \tag{17}$$

where r_{ii} is the radius of the conductor, measured in m; γ = 1.78107242 is Euler's constant; and $\ln\gamma$ = 0.577215665; e = 2.718281828 is the base of a natural logarithm.

Ratio (17) takes into account the alternating magnetic field of the current and the corresponding inverse current distribution in the ground. Similar to Formula (17), the expression for calculating the mutual impedance in the near range follows from Expression (14) when $i \ne k$ and $r \le 0.2$

$$\begin{gathered}\underline{Z}_{ik} = \tfrac{\omega\mu_0}{8} + j\tfrac{\omega\mu_0}{2\pi}\ln\left(\tfrac{1.85}{r_{ik}}\sqrt{\tfrac{\rho}{\omega\mu_0}}\right), \text{ Ohm}/m \\ r_{ik} = \sqrt{(x_i - x_k)^2 + (y_i - y_k)^2}\end{gathered} \tag{18}$$

where r_{ik} is the distance between the conductors i and k, measured in m.

For calculations in the intermediate range, it is advisable to transform Formula (14) to the following form:

$$\begin{aligned}\underline{F}_{ik} = 0.5 - \ln(\lambda r) - j\tfrac{\pi}{4} - \sum_{n=1}^{\infty} (-1)^n \tfrac{(r/2)^{2n}}{n!(n+1)!}\left[\cos\left(\tfrac{n\pi}{2}\right) + j\sin\left(\tfrac{n\pi}{2}\right)\right] \times \\ \times \left[[\ln(\lambda r) - m_n]\cos(2n\theta) - \theta\sin(2n\theta) + j\tfrac{\pi}{4}\cos(2n\theta)\right] - \\ -2\sum_{n=1}^{\infty} \tfrac{(-1)^n r^{2n-1}\cos[(2n-1)\theta]}{1^2\cdot 3^2\cdot\ldots\cdot(2n-1)^2\cdot(2n+1)}\left\{\cos\left[\tfrac{(2n-1)\pi}{4}\right] + j\sin\left[\tfrac{(2n-1)\pi}{4}\right]\right\}\end{aligned} \quad (19)$$

Formulas (13)–(19) are implemented in the Fazonord software package and prove valid in the near, intermediate, and far ranges.

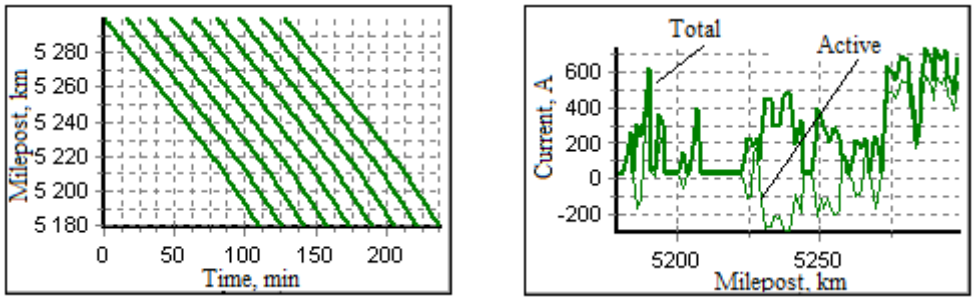
The following assumptions have been made when modeling the transformer:

- Stray inductance is taken into account by connecting an inductive component in series with the coil;
- The additional magnetic flux that makes a circuit through the tank walls of the transformer and determines the zero-sequence impedance is modeled by two additional rods of a five-rod transformer;
- The relationship between field strength and induction in the transformer core is assumed to be linear;
- The two outermost rods are characterized by the complex relative magnetic permeability $\underline{\mu}_{r1}{}' - j\underline{\mu}''_{r1}$; it can correspond to the magnetic permeability of the middle rods, or be taken equal to one to simulate the magnetic flux through the oil and the transformer tank. The cross-sectional areas of these rods are the same. Their lengths and magnetic permeabilities are equal to each other;
- The three middle rods of the magnetic core are characterized by a constant value of the complex magnetic permeability $\underline{\mu}_{r2}{}' - j\underline{\mu}''_{r2}$, determined from the nameplate values of current and no-load losses;
- Each coil has ohmic resistance and reactance $R_{ik} + jX_{ik}$, which are determined by the short-circuit parameters; here i is the winding number, which corresponds to the row of the matrix and k is the rod number minus one, or the phase number, which corresponds to the column of the matrix;
- The number of turns w_{ik} is determined by the effective inductance B_{2m} (T) in the core and the nominal voltage of the coil;
- The maximum number of transformer windings is assumed to be five.

The adequacy of the modeling was checked via comparison with the results of measurements performed at 220 kV substations feeding the traction networks of the main railway. The differences between the calculated and measured values of the asymmetry coefficients did not exceed 0.6%, and the differences in the values of the phase voltages did not exceed 2.3%.

The computational models were implemented in the Fazonord software package for nine cases. Eight cases corresponded to the COHL shown in Figure 4, and the other one to a standard power line, as shown in Figure 2. The models included the following components: five 220 kV power transmission lines, four traction substations (TS), and two sections of the contact system. We considered the passage of nine trains weighing 4084 tons (Figure 5a). Figure 5b shows the current profile, i.e., the current consumed by the electric locomotive as a function of the distance. Based on simulations, we determined the parameters defining the load flow and electromagnetic safety conditions. The dynamics of changes in some of them over time are shown in Figures 6–13. These figures show the time dependencies for the following parameters: voltage U on the bow collector of the first train; the unbalance ratio k_{2U} on 220 kV buses of TS 4; active power losses ΔP_{TN} in the traction network of the area between substations; active power losses in the transmission line 1 ΔP_{TL}; harmonic distortion k_{U220} at 220 kV buses of TS 4, phase C; harmonic distortion $k_{U27.5}$ at the 27.5 kV input of TS 4; amplitude $E_{\max}$ of electric field strength; amplitude $H_{\max}$ of magnetic field strength. For some transmission lines, these values were similar. Therefore, in order to

ensure the clarity of the graphical relationships, Figures 6–13 show curves for three lines: a 220 kV transmission line of conventional design, as well as COHLs with three-segment and concentric arrangements of conductors. Tables 1 and 2 show the extreme values of these parameters for all of the transmission lines considered.



(**a**) (**b**)

Figure 5. (**a**) Distance-time graph and (**b**) current profile of the train.

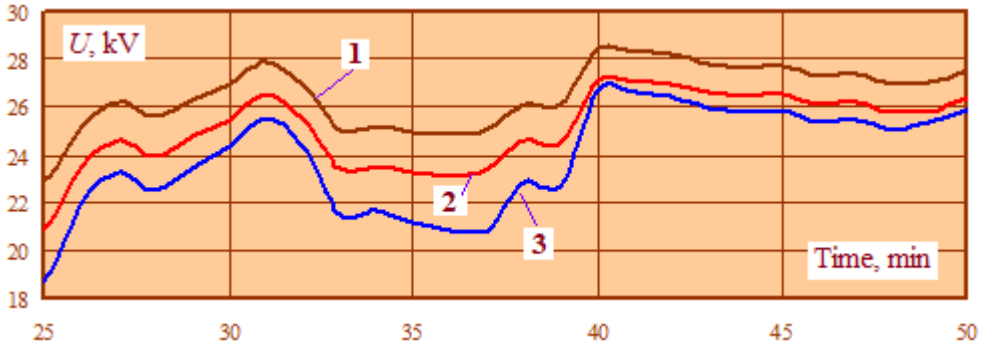


Figure 6. Voltage on the bow collector of the electric locomotive of the first train: 1 is COHL with a three-segment arrangement of conductors; 2 is COHL with a concentric arrangement of conductors; 3 is the transmission line of a conventional design with AS-600 conductors.

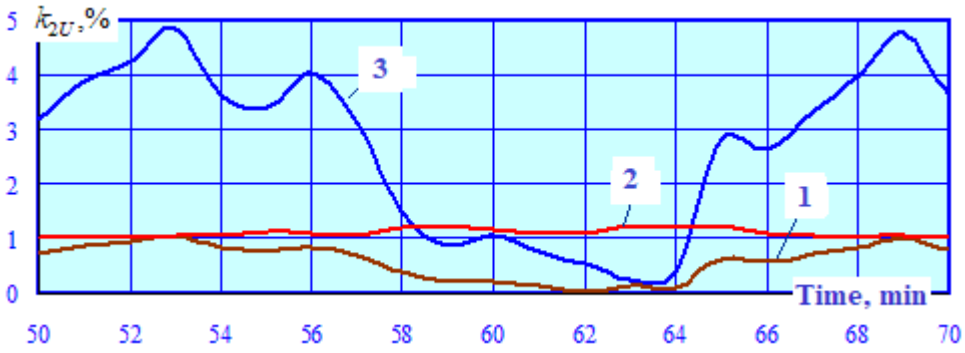


Figure 7. Negative sequence unbalance ratios at 220 kV buses of the TS—callout numbers correspond to those in Figure 6.

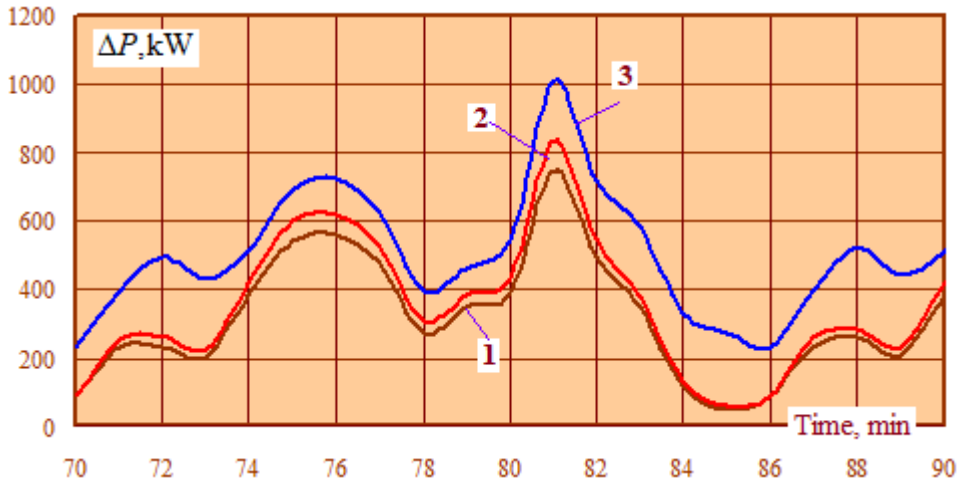


Figure 8. Power losses in the traction network of the middle inter-substation area—callout numbers correspond to those in Figure 6.

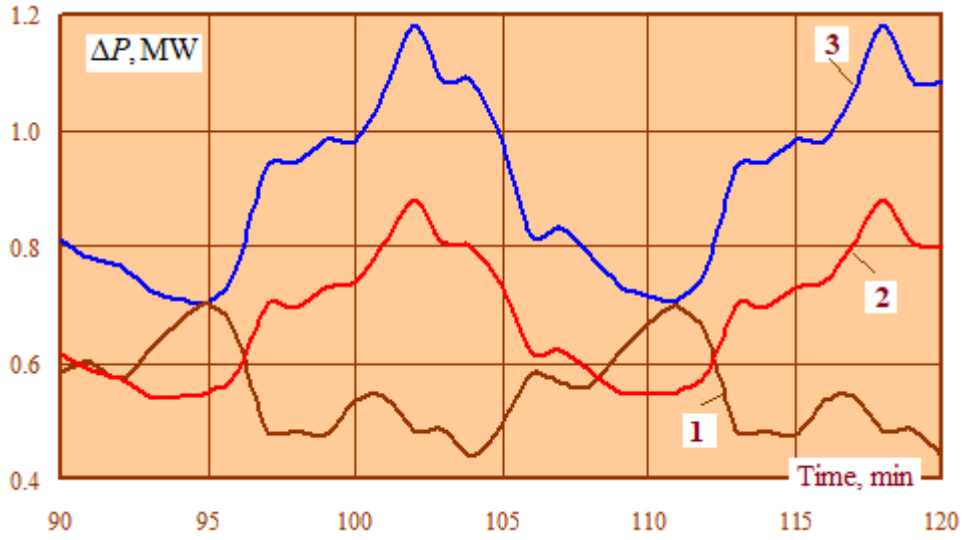


Figure 9. Power losses in the transmission line 1—callout numbers correspond to those in Figure 6.

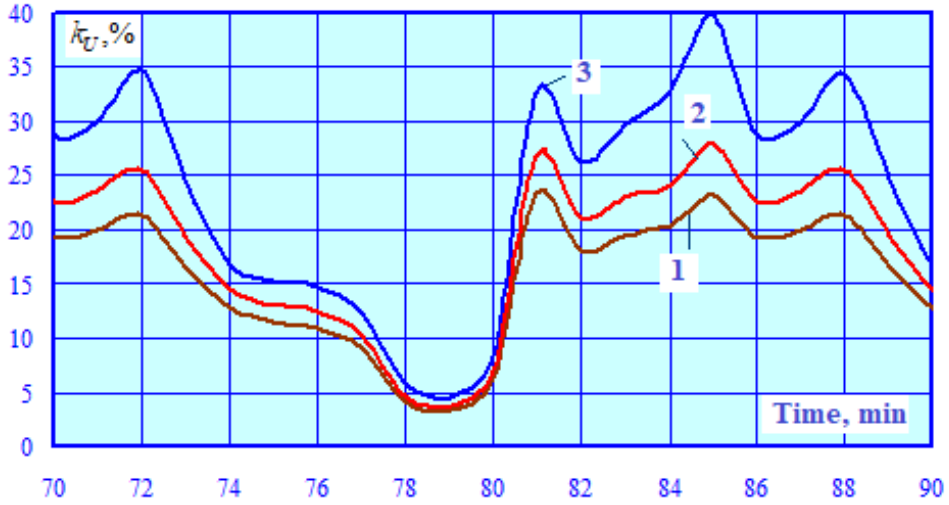


Figure 10. Total harmonic distortion values at the 27.5 kV input of TP 4—callout numbers correspond to those in Figure 6.

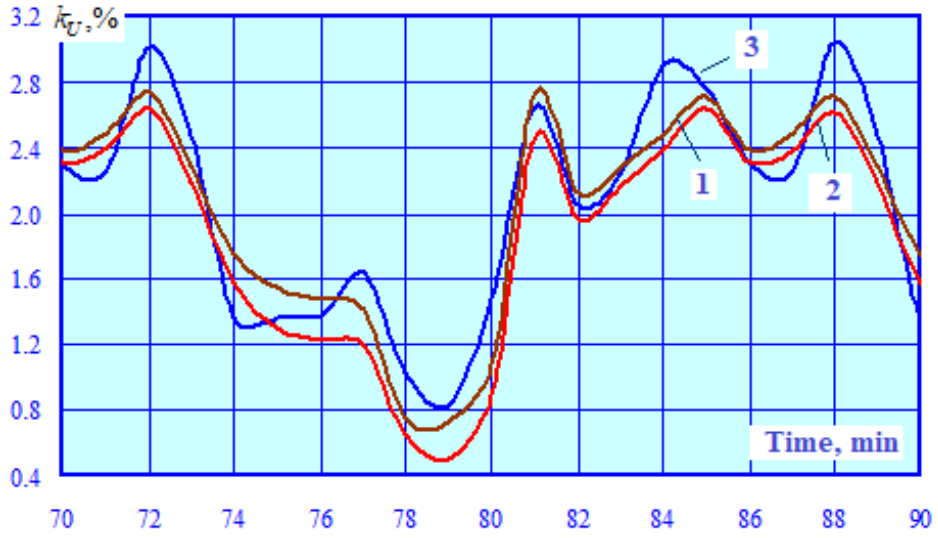


Figure 11. Total harmonic distortion values at 220 kV buses of TP 4, phase C—callout numbers correspond to those in Figure 6.

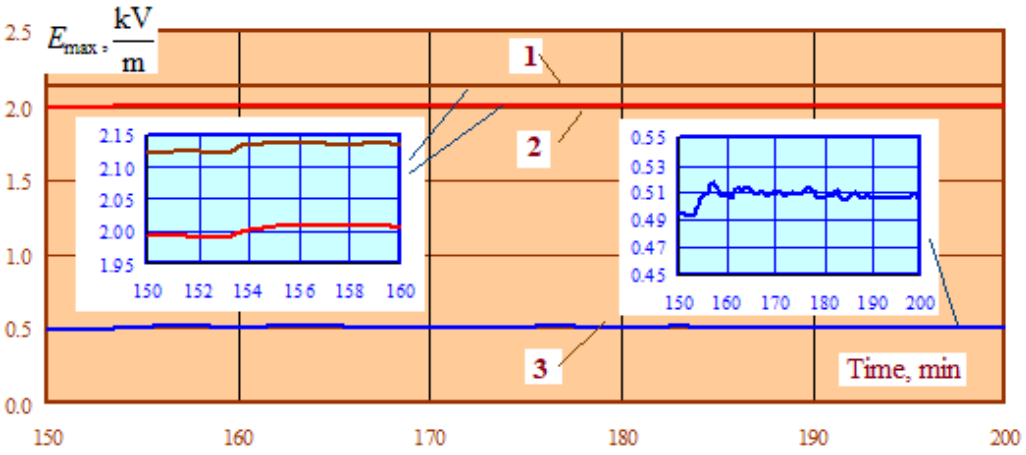


Figure 12. Electric field (EF) strength at a height of 1.8 m at the beginning of the transmission line 5.

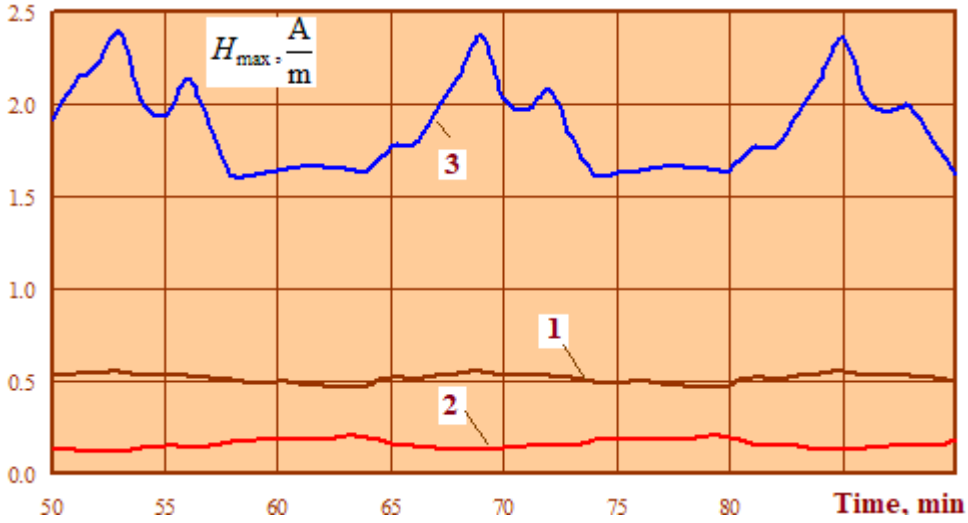


Figure 13. Magnetic field (MF) strength at a height of 1.8 m at the beginning of the transmission line 5—callout numbers correspond to those in Figure 6.

Table 1. Extreme values of parameters.

Transmission Line Design	U_{min}, kV	Max(k_{2U}), %	Max (ΔP_{TN}), kW	Max (ΔP_{TL}), MW
Standard power transmission line with AS-600 conductors	16.73	4.86	1015	1.18
COHL with a vertical arrangement of conductors	16.93	3.43	906	1.37
Coaxial two-segment COHL	18.24	2.1	872	1.18
Coaxial four-segment COHL	18.72	1.6	857	1.14
COHL with a delta arrangement of conductors	18.41	1.64	872	1.2
Double coaxial COHL	19.05	1.55	880	1.22
COHL with a parabolic arrangement of conductors	18.21	2.08	871	1.22
COHL with a three-segment arrangement of conductors	21.98	1.02	753	0.81
COHL with a concentric arrangement of conductors	19.76	1.37	832	0.88

Notes: U_{min} is the minimum voltage on the bow collector of the electric locomotive; k_{2U} is the unbalance ratio at 220 kV buses of TS 4; ΔP_{TN} represents power losses in the TN of the middle inter-substation area; 2; ΔP_{TL} represents losses in the transmission line 1.

Table 2. Maximum values of parameters.

Transmission Line Design	k_{U220}, %	$k_{U27.5}$, %	E_{max}, kV/m	H_{max}, A/m
Standard power transmission line with AS-600 conductors	3.17	39.74	0.52	2.39
COHL with a vertical arrangement of conductors	6.31	40.14	0.33	0.94
Coaxial two-segment COHL	4.05	33.19	0.92	0.66
Coaxial four-segment COHL	3.48	31.13	1.05	0.25
COHL with a delta arrangement of conductors	3.92	23.19	1.21	0.8
Double coaxial COHL	2.96	29.8	0.73	1.2
COHL with a parabolic arrangement of conductors	4.64	33.8	1.21	0.78
COHL with a three-segment arrangement of conductors	2.75	23.19	2.14	0.55
COHL with a concentric arrangement of conductors	2.68	27.87	2.01	0.22

Notes: k_{U220} is the harmonic distortion at 220 kV buses of TS 4, phase C; $k_{U27.5}$ is the harmonic distortion at the 27.5 kV input of TS 4; E_{max} is the amplitude of the electric field strength; H_{max} is the amplitude of the magnetic field strength.

Figure 6 depicts the dynamics of voltage change on the bow collector of the electric locomotive of the first train. Figure 7 shows similar plots for the negative-sequence unbalance ratios, which were calculated at 220 kV buses of the traction substation No. 4. Plots corresponding to the dynamics of changes in power losses in the traction network of the second inter-substation are shown in Figure 8. Similar dependencies for power losses in the transmission line 1 are shown in Figure 9. Figures 10 and 11 show the plots corresponding to harmonic distortion values in the feeder and traction networks. Figure 12 shows plots of the electric field strength at a height of 1.8 m at the beginning of the transmission line 5, and Figure 13 shows similar dependencies for the magnetic field. The spatial structure of the EMF strengths of a three-segment compact overhead line is illustrated in Figure 14.

A summary of the data characterizing the simulation results is shown in Tables 1 and 2 and Figures 15–24.

Our analysis of the results thus obtained allows us to conclude that the use of compact power transmission lines (Figure 4) instead of standard overhead lines (Figure 2) in the external power supply system of railroads enabled the following gains:

- Voltages on bow collectors of electrical rolling stock increased and stabilized (Table 1 and Figure 15). In the computational examples with a standard feeding line, voltage on the bow collector of the first train decreased below the permissible limit, and when using a three-segment COHL design it increased to 22 kV;
- Losses in the traction network were reduced; the maximum reduction took place when using a three-segment COHL design (Table 1 and Figure 17);
- Power quality was improved; negative-sequence unbalance ratios at 220 kV buses of traction substations were reduced (Table 1 and Figure 16);
- Harmonic distortions in the traction network (Table 2 and Figure 19) and at the interfaces with EPS networks (Table 2 and Figure 20) were reduced;
- The maximum amplitudes of the electric field (EF) of all the considered COHLs, except for the line with a vertical arrangement of wires, exceeded similar values for a standard power transmission line. The largest, fourfold, difference took place in the case of a three-segment COHL. However, the levels of EMF strengths for all the considered COHL designs did not exceed the permissible limits. Exceeding these limits only occurs when operating on a transmission line without de-energizing it (Figure 14).
- Design features of COHLs provided a reduction in the magnetic field (MF) strength of COHLs compared to power transmission lines of the standard design, Figure 22, Table 2. For example, the ratio of maximum MF amplitudes for a standard line and a concentric COHL reached 11.
- We observed the damping effects of COHLs, which manifested themselves as the reduction of field variability. The variation coefficients of EMF strengths for all of the considered COHLs were lower than those of the standard line (Figure 23). The maximum difference was observed for the double coaxial COHL and reached seven times. MF variability that was less than in the standard line took place in the case of the following designs (Figure 24): three- and two-segment lines, coaxial double lines, and a line with a vertical arrangement of conductors.

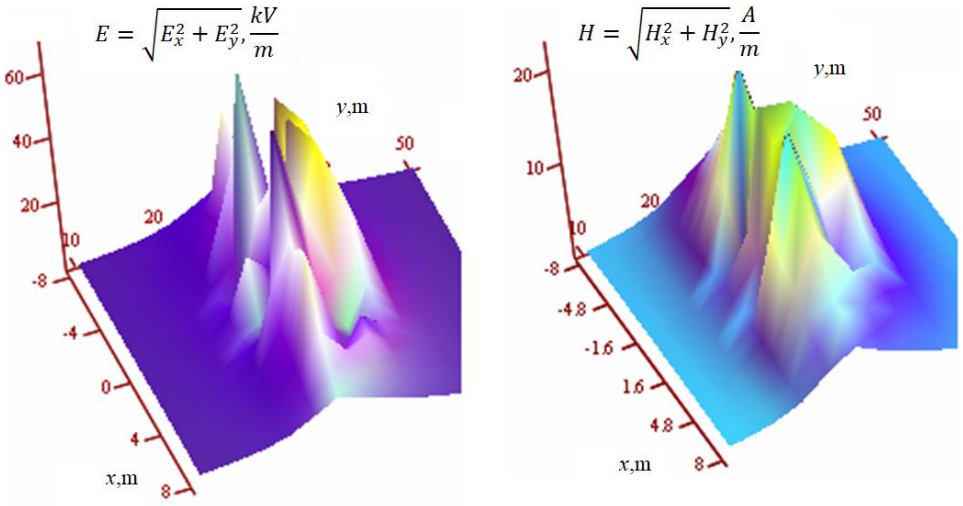


Figure 14. Spatial structure of the EMF strengths of a three-segment compact overhead line.

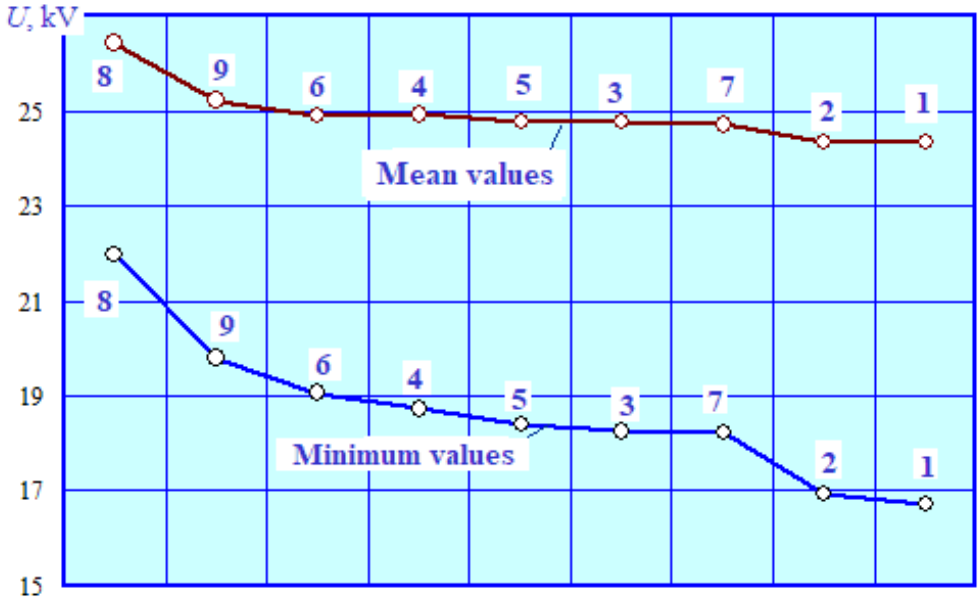


Figure 15. Voltage on the bow collector of the electric locomotive of the first train: 1 is a standard transmission line with AS-600 conductors; 2 is with a vertical arrangement of conductors; 3 represents a coaxial double-segment COHL; 4 is a coaxial four-segment COHL; 5 is a COHL with a delta arrangement of conductors; 6 is double coaxial COHL; 7 is a COHL with a parabolic arrangement of conductors; 8 is a COHL with a three-segment arrangement of conductors; 9 is a COHL with a concentric arrangement of conductors.

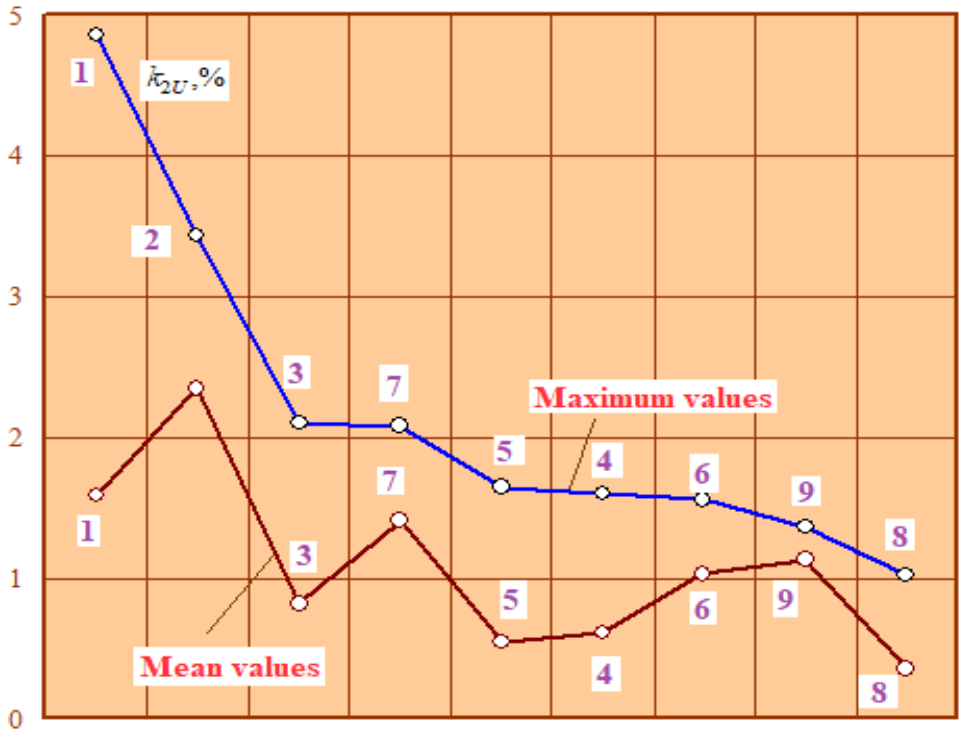


Figure 16. Negative-sequence unbalance ratios at 220 kV buses of TS 4—callout numbers correspond to those in Figure 15.

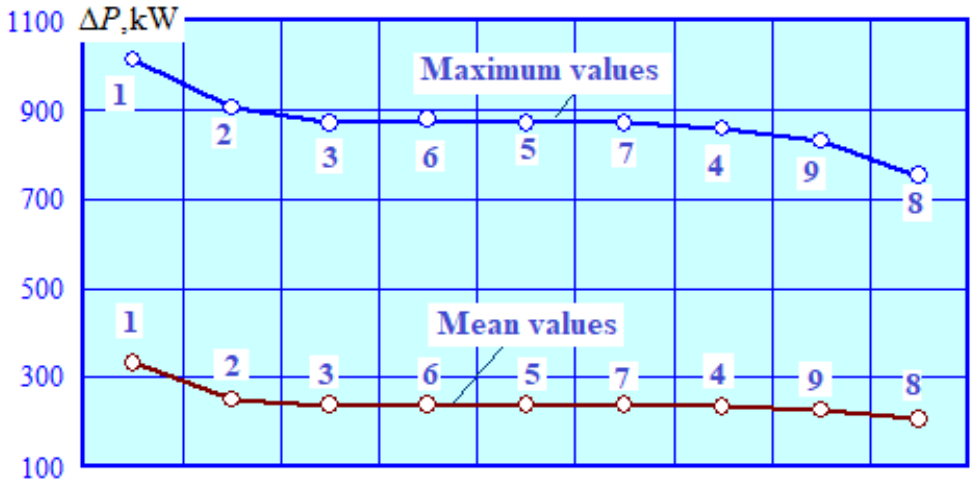


Figure 17. Power losses in the traction network of the middle inter-substation area—callout numbers correspond to those in Figure 15.

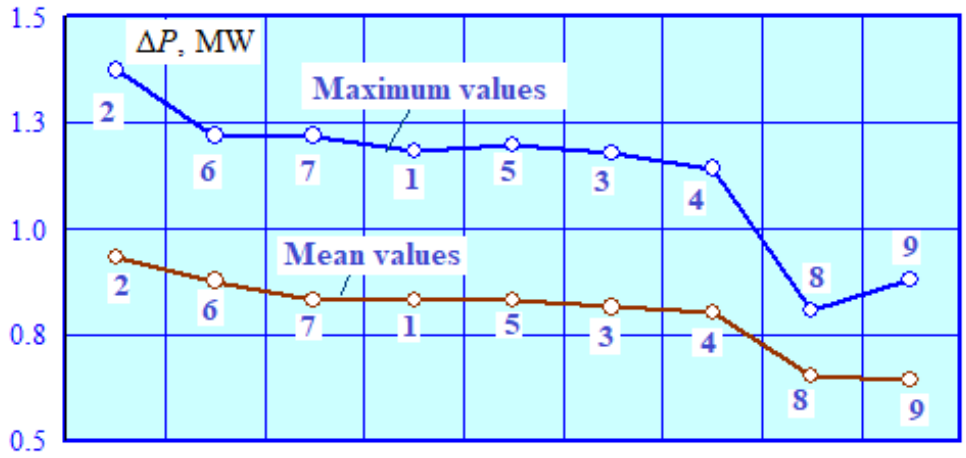


Figure 18. Power losses in the transmission line 1: callout numbers correspond to those of Figure 15. Total cross-sections of conductors differ slightly across all transmission lines.

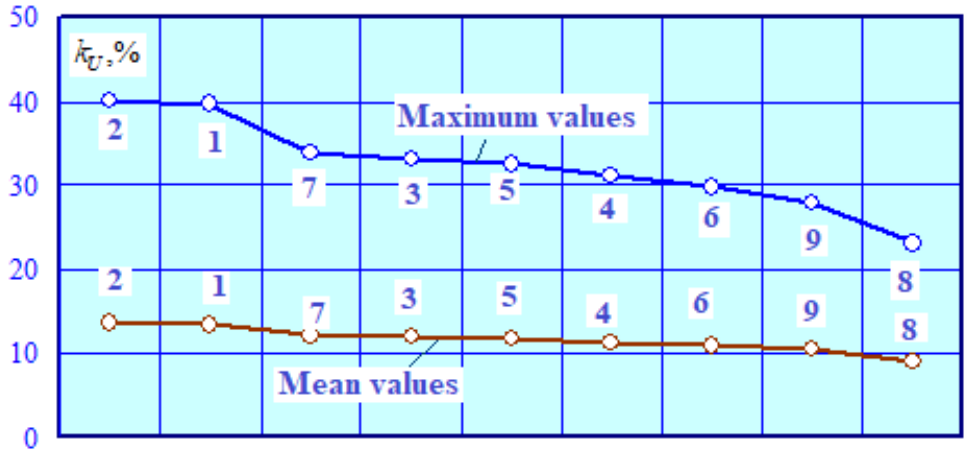


Figure 19. Total harmonic distortion values at the 27.5 kV input of TS No. 4—callout numbers correspond to those in Figure 15.

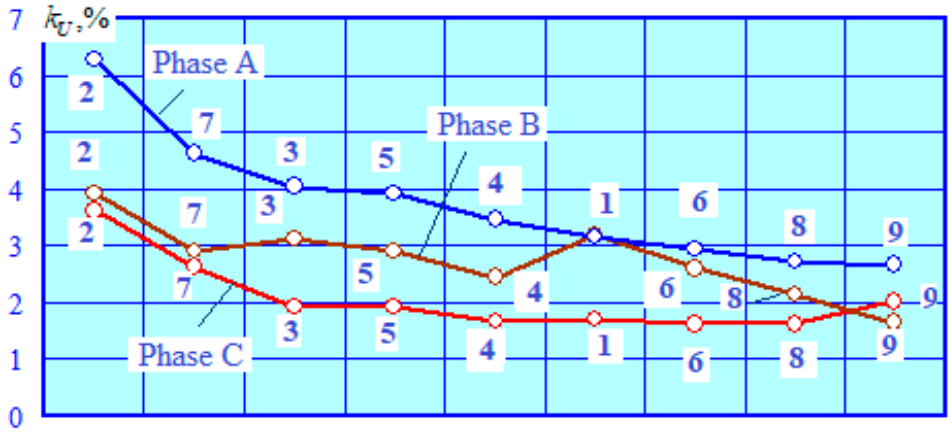


Figure 20. Maximum total harmonic distortion values at 220 kV buses of TS No. 4—callout numbers correspond to those in Figure 15.

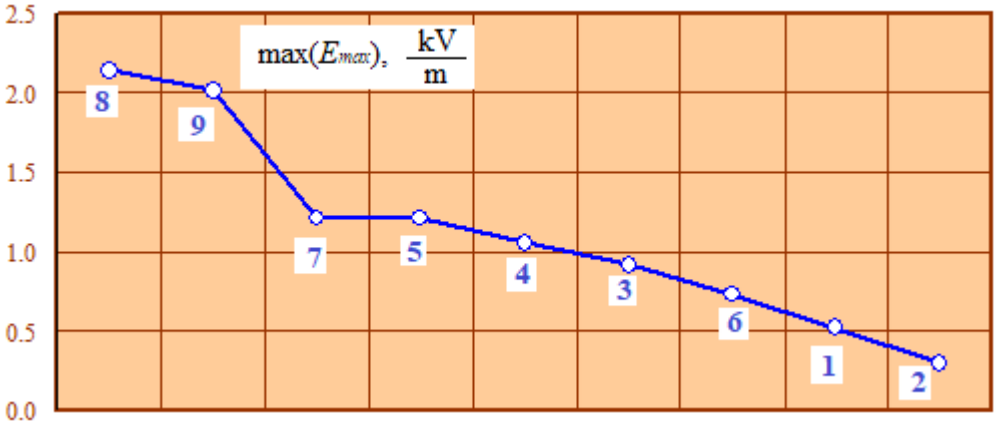


Figure 21. Maximum amplitudes of the electric field at the starting end of the transmission line 5—callout numbers correspond to those in Figure 15.

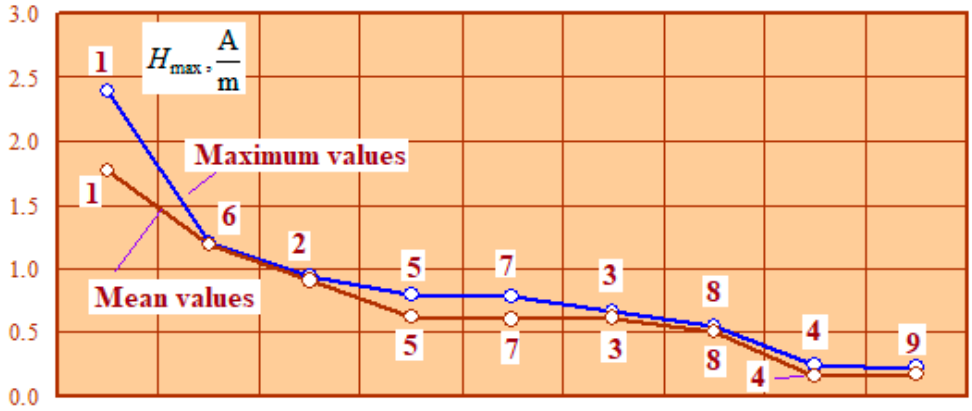


Figure 22. Maximums and mean values amplitudes of the magnetic field at the starting end of the transmission line 5—callout numbers correspond to those in Figure 15.

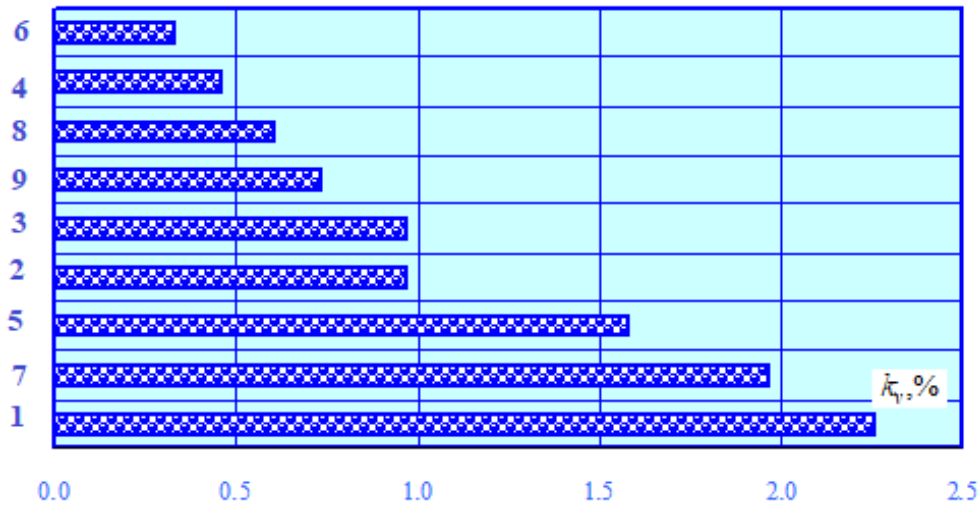


Figure 23. Coefficients of variation of amplitudes of electric field strengths: $k_v = \frac{\sigma}{\overline{E}_{\max}}$; σ is the standard deviation; $\overline{E}_{\max}$ is the mean value of the EF amplitude—the callout numbers correspond to those of Figure 15.

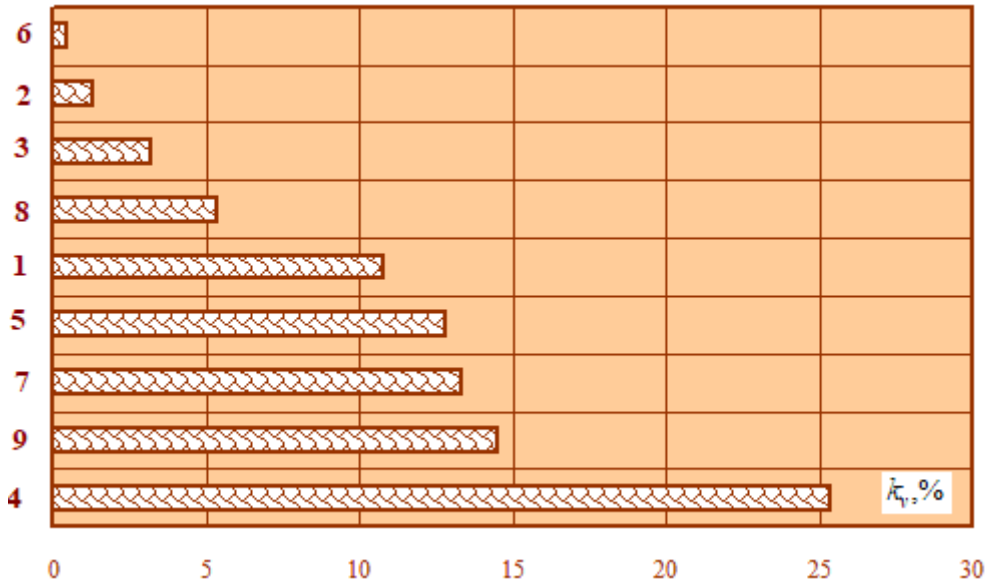


Figure 24. Coefficients of variation of magnetic field amplitudes—the callout numbers correspond to those of Figure 15.

4. Conclusions

We have developed a workflow for the digital modeling of unbalanced and non-sinusoidal power flows, as well as that of electromagnetic fields of power supply systems of railroads, the external network of which represents compact power transmission lines of different designs. Based on our simulation results, we can conclude that compact power transmission lines with three-segment and concentric arrangements of conductors scored best in terms of power quality and energy efficiency. However, the designs of such transmission lines are quite complex and entail higher construction costs.

We have proposed a technique for determining the EMF strength of compact overhead lines that power traction substations. To that end, eight COHL designs have been considered.

The models developed by the authors for load flow analysis and EMF of COHLs are versatile, and they can be extended to COHLs of any type. Their use in the practice of

designing external power supply systems for railroads will be instrumental to making informed decisions on the choice of rational designs of high-voltage power transmission lines.

The proposed models of power systems and power supply systems for railroads enable the evaluation of efficacy and application of COHLs for power supply of traction substations. The approach detailed in the article stands apart from other research in that it is systems-based and treats COHLs as inseparable from a complex power system. In contrast to traditional methods based on a single-line representation, our models were built using the three-phase (ABC) reference frame, which provides the most adequate modeling of power system load flows with single-phase traction loads that create significant unbalances in the electrical networks that feed them. The simulation took into account the dynamics of changes in traction loads by simulating the movement of trains along real-world rail track profiles.

Author Contributions: Conceptualization, K.S. and A.K.; methodology, A.K., I.F., E.V. and K.S.; software, A.K.; validation A.K., I.F., E.V. and K.S.; formal analysis, I.F. and E.V.; investigation, A.K., I.F., E.V. and K.S.; resources, K.S.; data curation, A.K., I.F., and E.V.; writing—original draft preparation, A.K., I.F., and E.V.; writing—review and editing, A.K. and K.S.; visualization, A.K., I.F., and E.V.; supervision, A.K.; project administration, A.K. and K.S.; funding acquisition, K.S. All authors have read and agreed to the published version of the manuscript.

Funding: The research was carried out under State Assignment No. "Applied Scientific Research" for "Development of methods, algorithms, and software for modeling load flows of DC traction power supply systems and electromagnetic fields in traction substations of AC railroads".

Institutional Review Board Statement: Not applicable.

Informed Consent Statement: Not applicable.

Data Availability Statement: Data sharing not applicable. No new data were created or analyzed in this study. Data sharing is not applicable to this article.

Conflicts of Interest: The authors declare no conflict of interest.

References

1. Aleksandrov, G.N. *Operating Conditions of Overhead Power Transmission Lines*; Energy Industry Training Center (TsPKE): Saint Petersburg, Russia, 2006; 139p. (In Russian)
2. Douglass, J.; Stewart, D. Introduction to Compact Lines. In *EPRI Transmission Line Reference Book—115–345kV Compact Line Design*; Electric Power Research Institute: Washington, DC, USA, 2008.
3. Surianu, F.-D. Determination of the induced voltages by 220 kV electric overhead power lines working in parallel and narrow routes. Measurements on the ground and mathematical model. *WSEAS Trans. Power Syst.* **2009**, *4*, 264–274.
4. Zarudsky, G.K.; Samalyuk, Y.S. On considerations related to power flows of 220 V compact overhead power lines. *Elektrichestvo* **2013**, *5*, 8–13. (In Russian)
5. Lavrov, Y.A.; Voitovich, R.A.; Petrova, N.F. Considerations in construction of high-voltage compact overhead power transmission lines. In *Science in Russia: Promising Research and Development*; Publishing house CRNS: Novosibirsk, Russia, 2017; pp. 152–159. (In Russian)
6. Plotnikov, V.V.; Vasilenko, N.E.; Protasenko, I.S.; Zuev, M.M.; Zueva, T.S.; Zakutsky, V.I.; Glushkin, S.V.; Ermolov, N.S. Use of compact lines as one of the means to increase transmission capacity. *Potential Mod. Sci.* **2016**, *4*, 37–43. (In Russian)
7. Postolaty, V.; Bycova, E.; Berzan, V. Compact and Controllable Electric Lines. In Proceedings of the 2019 International Conference on Electromechanical and Energy Systems (SIELMEN), Craiova, Romania, 9–11 October 2019.
8. Seliverstov, G.I.; Komar, A.V.; Petrenko, V.N. Designs and parameters of compact single-circuit power transmission lines with concentric arrangement of phase conductors. *ENERGETIKA* **2012**, *6*, 41–45. (In Russian)
9. Stepanov, V.M.; Karnitsky, V.Y. Compact power transmission lines. *Izv. TulGU. Tekhnicheskie Nauki.* **2010**, *3–5*, 49–51. (In Russian)
10. Fedin, V.T. *Innovative Engineering Solutions in Power Transmission Systems*; Publishing house BNTU: Minsk, Belarus, 2012; 222p. (In Russian)
11. Shakarian, Y.G.; Timashova, L.V.; Kareva, S.N. Efficiency of electric power transmission by compact controlled overhead lines. *Energiya Edinoy Seti.* **2014**, *3*, 4–15. (In Russian)
12. Postolaty, V.M.; Bykova, E.V.; Suslov, V.M.; Shakaryan, Y.G.; Timashova, L.V.; Kareva, S.N. Efficiency of compact controlled high-voltage power lines. *Probl. Reg. Energetics* **2015**, *3*, 1–17. (In Russian)
13. Hartono, J.; Ridwan, M.; Mafruddin, M.M.; Habibi, H.; Anugrahany, E. 500 kV quadruple circuit compact transmission line redesign study to reduce the impact of lightning strikes. In Proceedings of the 2021 3rd International Conference on High Voltage Engineering and Power Systems (ICHVEPS), Bandung, Indonesia, 5–6 October 2021.

14. Jing, C.; Shanshan, Q.; Jinxiang, L.; Xiong, W.; Zongren, P. Research of Grading Ring for High Altitude 500 kV Compact Transmission Line. In Proceedings of the 2018 IEEE International Conference on High Voltage Engineering and Application (ICHVE), Athens, Greece, 10–13 September 2018.
15. Buryanina, N.S.; Koroluk, Y.F.; Timofeeva, A.-M.V. 35–200 kV Compact Transmission Lines with Improved Power Transfer Capability. In Proceedings of the 2020 International Multi-Conference on Industrial Engineering and Modern Technologies (FarEastCon), Vladivostok, Russia, 6–9 October 2020.
16. Shu, R.; Wei, H.; Fan, Y.; Jianbin, C.; Zhi, L. A novel equilvalent model to analyze the influence between the parallel UHVDC and EHVAC transmission lines. In *2010 Conference Proceedings IPEC*; IEEE: Piscataway, NJ, USA, 2010.
17. Buryanina, N.; Korolyuk, Y.; Koryakina, M.; Suslov, K.; Lesnykh, E. Compact Power Transmission Lines. In Proceedings of the 2019 International Multi-Conference on Industrial Engineering and Modern Technologies (FarEastCon), Vladivostok, Russia, 1–4 October 2019. [CrossRef]
18. Dahab, A.A.; Amoura, F.K.; Abu-Elhaija, W.S. Comparison of magnetic-field distribution of noncompact and compact parallel transmission-line configurations. *IEEE Trans. Power Deliv.* **2005**, *20*, 2114–2118. [CrossRef]
19. Ordon, T.J.F.; Lindsey, K.E. Considerations in the design of three phase compact transmission lines. In Proceedings of the ESMO'95—1995 IEEE 7th International Conference on Transmission and Distribution Construction, Operation and Live-Line Maintenance, Columbus, OH, USA, 29 October–3 November 1995.
20. Khayam, U.; Prasetyo, R.; Hidayat, S. Electric field analysis of 150 kV compact transmission line. In Proceedings of the 2017 International Conference on High Voltage Engineering and Power Systems (ICHVEPS), Denpasar, Indonesia, 2–5 October 2017.
21. Xiao, B.; Wu, T.; Liu, T.; Liu, K.; Peng, Y.; Su, Z.; Tang, P.; Lei, X. Experimental investigation on the minimum approach distance for live working on 1000kV UHV compact transmission line. In Proceedings of the In Proceedings of the 2016 IEEE International Conference on High Voltage Engineering and Application (ICHVE), Chengdu, China, 19–22 September 2016.
22. Chai, X.; Liang, X.; Zeng, R. Flexible compact AC transmission system—A new mode for large-capacity and long-distance power transmission. In Proceedings of the 2006 IEEE Power Engineering Society General Meeting, Montreal, QC, Canada, 18–22 June 2006.
23. Mohajeryami, S.; Doostan, M. Investigating the lightning effect on compact transmission lines by employing Monte Carlo method. In Proceedings of the 2016 IEEE/PES Transmission and Distribution Conference and Exposition (T&D), Dallas, TX, USA, 3–5 May 2016.
24. Khayam, U.; Prasetyo, R.R.; Hidayat, S. Magnetic field analysis of 150 kV compact transmission line. In Proceedings of the 2017 International Conference on High Voltage Engineering and Power Systems (ICHVEPS), Denpasar, Indonesia, 2–5 October 2017.
25. de Melo, M.O.B.C.; Fontana, E.; Fonseca, L.C.; Naidu, S. Lightning Protection of Compact Transmission Lines. In Proceedings of the June Conference: International conference on power systems transients, Seattle, WA, USA, 22–26 June 1997.
26. Smith, D.C. Power line carrier system on a 400 kV compact delta transmission line. *Trans. South Afr. Inst. Electr. Eng.* **2001**, *92*, 16–23.
27. Gong, X.; Wang, H.; Zhang, Z.; Wang, J.; Wang, J.; Yuan, Y. Tests on the first 500 kV compact transmission line in China. In Proceedings of the PowerCon 2000—2000 International Conference on Power System Technology, Perth, WA, Australia, 4–7 December 2000.
28. Wei-Ming, M. The power characteristic of 500 kV large power compact overhead transmission line. In Proceedings of the TENCON'93—IEEE Region 10 International Conference on Computers, Communications and Automation, Beijing, China, 19–21 October 1993.
29. Bin, Z.; Wenhui, C.; Jiayu, H. Typical models of compact transmission lines and application prospect in 500 kV AC system of China. In Proceedings of the POWERCON'98. 1998 International Conference on Power System Technology, Beijing, China, 18–21 August 1998.
30. Varivodov, V.N. Compact power transmission lines. *Elektro* **2006**, *2*, 2–6. (In Russian)
31. Kryukov, A.; Suslov, K.; Van Thao, L.; Hung, T.D.; Akhmetshin, A. Power Flow Modeling of Multi-Circuit Transmission Lines. *Energies* **2022**, *15*, 8249. [CrossRef]
32. Bulatov, Y.; Kryukov, A.; Suslov, K. Integrated Modeling of the Modes of High Voltage Long Distance Electricity Transmission Lines. In Proceedings of the 2022 9th International Conference on Electrical and Electronics Engineering (ICEEE), Alanya, Turkey, 29–31 March 2022; pp. 45–49. [CrossRef]
33. Zakaryukin, V.P.; Kryukov, A. *Complex Unbalanced Load Flows of Electrical Systems*; Publishing House of Irkutsk State University: Irkutsk, Russia, 2005; 273p. (In Russian)
34. Zakaryukin, V.P.; Kryukov, A.V.; Le Van, T. *Complex Modeling of Multi-Phase, Multi-Circuit, and Compact Power Transmission Lines*; Irkutsk State Transport University (IrGUPS): Irkutsk, Russia, 2020; 296p. (In Russian)
35. Carson, I.R. Wave propagation in overhead wires with ground return. *Bell Syst. Tech. J.* **1926**, *5*, 539–554. [CrossRef]

Disclaimer/Publisher's Note: The statements, opinions and data contained in all publications are solely those of the individual author(s) and contributor(s) and not of MDPI and/or the editor(s). MDPI and/or the editor(s) disclaim responsibility for any injury to people or property resulting from any ideas, methods, instructions or products referred to in the content.